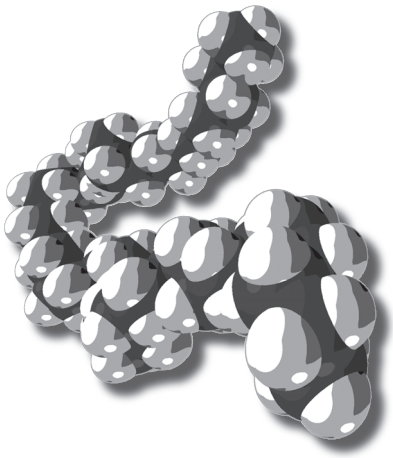

Macromolecular Materials and Engineering

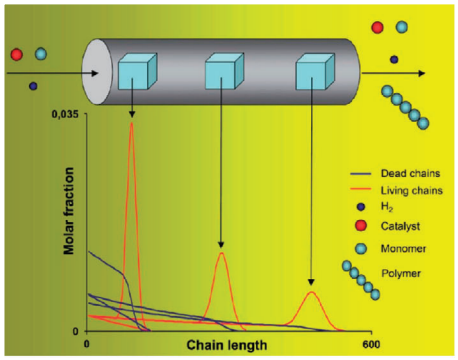

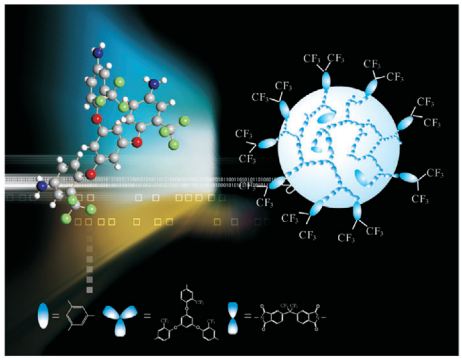

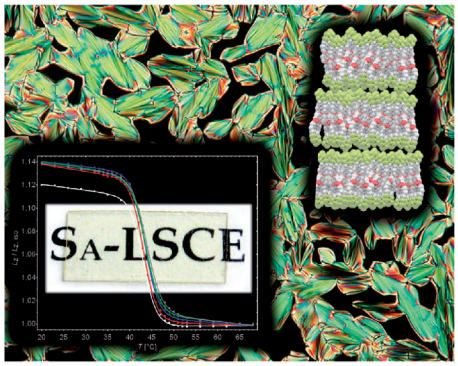

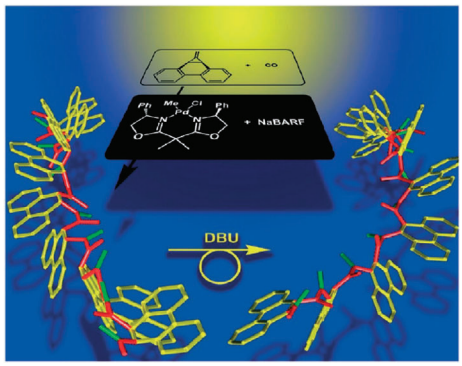

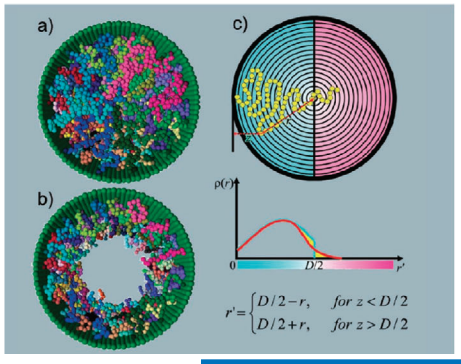

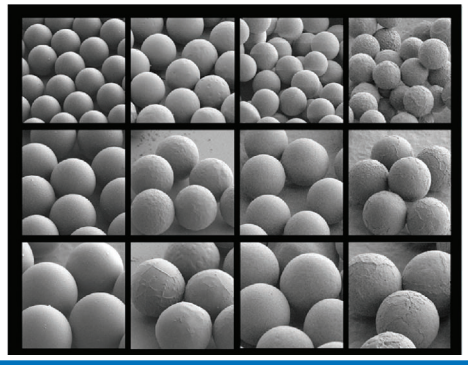

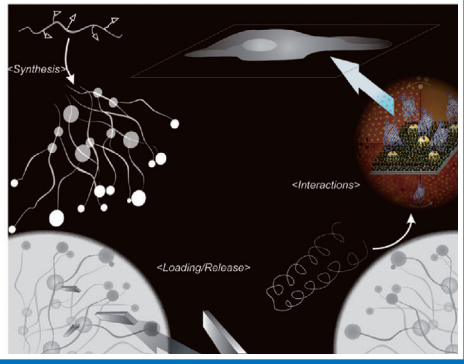

Reprints

WILEY-VCH

Percolated Network Structure Formation and Rheological Properties in Nylon 6/Clay Nanocomposites

Chihiro Mizuno, Baiju John, Masami Okamoto*

To understand the effect of the percolated clay network structure formed by the exfoliated clay layers in nanocomposites, the clay network structure in nylon-6-based nanocomposites is characterized using TEM and FFT analyses. A MMT volume fraction between 0.013 and 0.014 is the percolation threshold for strong network formation. The volume spanning MMT network leads to a very high flow activation energy as compared with that of neat nylon 6, resulting in the pseudo-solid like response under molten state in N6CNs. A canonical NVT-MD simulation was conducted in the system made up by nylon 6 molecules/$Si(OH)_4$ molecules. The formation of the strong interfacial interaction between nylon 6 molecules and $Si(OH)_4$ molecules induced by OH groups is suggested.

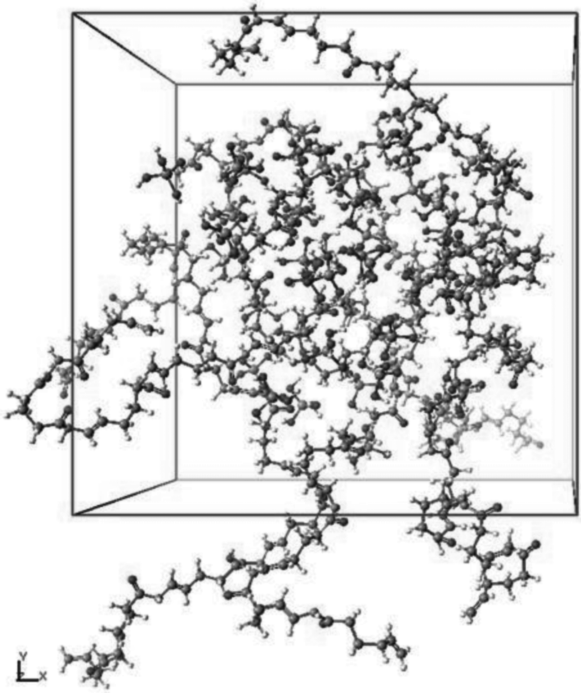

1. Introduction

A decade of research has shown that nanostructured materials have the potential to significantly impact growth at every level of the world economy in the 21st century. Of particular interest is recently developed nanocomposites consisting of a polymer and layered silicate because they often exhibit remarkably improved mechanical and various other properties[1–6] as compared with pure polymer or conventional composites (both micro- and macrocomposites). These concurrent property improvements are well beyond what can be generally achieved through the micro-/macrocomposites preparation.

A primary progress in polymer/layered silicate nanocomposites, a Nylon 6/layered silicate hybrid[7] reported by Toyota Central Research & Development Co. Inc. (TCRD), was successfully prepared by in situ polymerization of ε-caprolactam in a dispersion of montmorillonite (MMT). The silicate can be dispersed in liquid monomer or a solution of monomer. It has also been possible to melt-mix polymers with layered silicates, avoiding the use of organic solvents. The latter method permits the use of conventional processing techniques such as injection molding and extrusion. This new class of material is now being

C. Mizuno, B. John, M. Okamoto
Advanced Polymeric Nanostructured Materials Engineering, Graduate School of Engineering, Toyota Technological Institute, 2-12-1 Hisakata, Tempaku, Nagoya 468-8511, Japan
E-mail: okamoto@toyota-ti.ac.jp

DOI: 10.1002/mame.201200065

introduced in structural applications, such as gas barrier film and other load-bearing applications.[5]

Polymer/clay nanocomposites (PCNs) and their self-assembly behaviors have recently been approached to produce nanoscale polymeric materials.[1–6] Additionally, these nanocomposites have been proposed as model systems to examine polymer structure and dynamics in confined environments.[8–10]

In order to understand the processability of these materials (i.e., the final stage of any polymeric material), one must understand the detailed rheological behavior of these materials in the molten state. Understanding the rheological properties of PCN melts are not only important in gaining a fundamental knowledge of the processability but is also helpful in understanding the structure-property relationships in these materials. Although rheological measurement is indirect probe, they are a well-established approach to probe the interaction between nanofiller and polymer matrix and the time-dependent structure development. In addition, more clear nanoscale and mesoscale structure development of the systems could be provided when combined with X-ray/light scattering experiments and electron microscopy.

The original mesoscale structure in PCNs consists of randomly oriented exfoliated layers or tactoids of layers. This randomly distributed nanofiller forms a "organo-clay network" structure, which is mediated by polymer chains and organo-clay-organo-clay interactions. This meso-structure, which is intrinsically disordered metastable state and out of equilibrium, offers an apt analogy to soft colloidal glasses and gels.[11,12]

Ren et al.[13] discussed the analogy to the dynamics of soft colloidal glasses, exhibiting yield stress, thixotropy, and slow stress recovery under deformation.[12,14] A glass is homogenious on interparticle structure with elasticity derived from caging effect, which is characterized by long-range electrostatic repulsion and short-range attraction.[14] In the colloidal solid, the storage modulus and complex viscosity show logarithmic dependence time. For example, in an aqueous Laponite dispersion, the structure reorganization responsible for the rheological behavior depend upon the ionic strength of the dispersion, which balances the attractive and repulsive forces between clay domains.

On the other hand, a gel also shows the soft glassy dynamics, which is associated with metastable, structural heterogeneity on mesoscale length, caused by a percolation infinite (volume spanning) network. PCNs have a structural hierarchy without long-range repulsive interaction, leaving short-range attractive forces (van der Waals force) between polymer and clay because of the surface modification of clay by cationic intercalant. For this reason, PCN melts was classified as an attractive colloidal gels.[11]

The existence of percolated clay network structure, which is ignored in many literatures as always, is responsible for the linear viscoelastic response observed in PCN melts. The main objective of this study is to prove the effect of the percolated clay network structure formed by the randomly oriented exfoliated clay layers in PCNs on both solid and melt rheological properties. For this purpose, we first examined fast Fourier transform (FFT) analysis on digitally saved images of transmission electron microscope (TEM) micrographs using the image analysis, which allowed to provide us information equivalent to the scattering analyses. Using a molecular mechanics/molecular dynamics (MM/MD) program, we examined the dynamics of polymer chains in confined environment. We discussed the interfacial interaction between nylon 6 molecules and silicate particles, and calculated the potential and kinetic energies.

2. Experimental Section

2.1. Materials

The nylon-6-based nanocomposites (N6CNs) were kindly supplied by Dr. A. Usuki of Toyota Central R&D Labs., Inc. It was synthesized by in situ polymerization of ε-caprolactam in lauryl ammonium intercalated MMT in the presence of small amount of 6-aminocaproic acid (the number- and weight-average molecular weights $\overline{M}_n$ and $\overline{M}_w$ of N6CNs are 19.7×10^3 and 45.0×10^3 g mol^{-1}, respectively).[15] The different amounts of inorganic MMT part, obtained from the burning out of organic part, were 1.6 and 3.7 wt% and are designated as N6C1.6 and N6C3.7. The $\overline{M}_n$ and $\overline{M}_w$ of pure nylon-6 polymerized in bulk are 21.7×10^3 and 44.0×10^3 g mol^{-1}, respectively.

The dried nylon 6 and N6CNs pellets were then converted into sheets with a thickness of 0.8–1.0 mm by pressing with ≈1 MPa at 250 °C for 2 min using a hot press. The molded sheets were then quickly quenched between glass plates and then annealed at 50 °C for 2 h to crystallize isothermally before being subjected to characterizations.

2.2. Transmission Electron Microscopy (TEM)

Nanoscale structure of N6CNs were investigated by means of TEM (H-7100, Hitachi Co.), operating at an accelerating voltage of 100 kV. The ultra thin sections (the edge of the sample sheet perpendicular to the compression mold) with a thickness of 80 nm were microtomed at −80 °C using a Reichert Ultra cut cryo-ultramicrotome after suitably staining the sample with 12 tungstophosphoric acid at 80 °C for 2 h.

2.3. Fast Fourier Transform (FFT)

For analyzing the features of the micrographs, we carried out FFT analysis on digitally saved images of TEM micrographs using the commercial image analysis software (Ultimage®, Graftek,

France),[16] which allowed to provide us information equivalent to the scattering analyses.

2.4. Melt Rheology

Melt rheological measurements were conducted on a RDAII instrument with a torque transducer capable of measurements in the range of 0.2–200 g cm. Dynamic oscillatory shear measurements were performed by applying a time dependent strain of $\gamma(t) = \gamma_o \sin(\omega t)$, where γ_o is the strain amplitude, ω is the frequency, and t is the time. The resultant shear stress is $\sigma(t) = \gamma_o [G' \sin(\omega t) + G'' \cos(\omega t)]$, with G' and G'' being the storage and loss modulus, respectively. Measurements were conducted by using a set of 25 mm diameter parallel plates with a sample thickness of ~0.8 mm and in the temperature range of 225–255 °C. The strain amplitude was fixed to 15% for nylon 6 and 10% for N6CNs, respectively, to obtain reasonable signal intensities even at elevated temperature or low frequency (ω) to avoid the nonlinear response. For each sample investigated, the limits of linear viscoelasticity were determined by performing strain sweeps at a series of fixed ω's. The master curves were generated using the principle of time-temperature superposition and shifted to a common reference temperature (T_r) of 235 °C, which was chosen as the most representative of a typical processing temperature of nylon 6.

2.5. Dynamic Mechanical Analysis (DMA)

Dynamic mechanical properties of nylon 6 and N6CN samples ($35 \times 12 \times 0.8$ mm^3 = width × length × thickness) were measured using RDAII in the tension-torsion mode. The temperature dependence of dynamic storage modulus (G') and tan δ of the samples were measured at a constant frequency (ω) of 6.28 rad s^{-1}, a strain amplitude of 0.05%, and in the temperature range of −150–200 °C with a heating rate of 2 °C min^{-1}. The thermal expansion coefficient (α) in °C is calculated by Equation 1:

$$\alpha = \frac{\Delta L}{\Delta T} \frac{1}{L_0} \quad (1)$$

where ΔL is the change in length in mm, ΔT is the change in temperature, and L_0 is the original length of the sample (=35 mm). The value of α is selected in the temperature range of −150–20 °C because of the glass transition temperature of the samples were observed above 25 °C.

2.6. Differential Scanning Calorimetry (DSC)

The crystallized specimens were characterized by using temperature-modulated DSC (TMDSC) (TA 2920; TA Instruments) at the heating/cooling rate of 5 °C min^{-1} with a heating/cooling cycle of the modulation period of 60 s and an amplitude of ±0.769 °C, to determine the melting temperature (T_m) and heat of fusion (ΔH), the DSC was calibrated with Indium before experiments. For the measurement of degree of crystallinity (χ_c) prior to TMDSC analysis, the extra heat absorbed by the crystallites formed during heating had to be subtracted from the total endothermic heat flow due to the melting of the whole crystallites. This can be done according to the principles and procedures described in our previous paper.[17] By considering the melting enthalpy of 100% crystalline nylon 6 (α-phase as 241 J g^{-1} and γ-phase as 239 J g^{-1}, respectively[18]), we have estimated the value of the χ_c of neat nylon 6 and N6CNs, and these values are also presented in Table 1.

Table 1. TMDSC properties and thermal expansion coefficient (α) of neat nylon 6 and its nanocomposite.

Sample	T_m [°C]	ΔH [J g^{-1}]	χ_c [%]	α [°C]
nylon 6	221.4	70.5	29.5	10.75×10^{-5}
N6C1.6	211.7	52.6	22.0	9.42×10^{-5}
N6C3.7	210.9	50.5	21.1	8.84×10^{-5}

2.7. Computer Simulation

Using MM program (MM2 Scigress, ver 2.2.0, Fujitsu Ltd.) we proposed the molecular structures of monomer, nylon 6, and silicate by taking their van der Waals radii into account. Optimization of the molecular structure was based on the minimization of the total energy of the molecular system. We conducted the canonical (constant particle number N, volume V, and temperature T) MD simulation at 298 K using a MD program (Scigress, ver 2.2.0, Fujitsu Ltd.), and calculated the enthalpy (interfacial interaction), potential and kinetic energies. The product run of equilibrium MM/MD simulation was then executed for 100 ps with a time step of 0.2 fs. In all MD simulation, the atoms with non-bonding have the dispersive interaction described by Lennard-Jones (LJ) van der Waals potential. The most crucial and important aspect of these calculations is the method selected for sampling the relevant configurational phase space. Accordingly, the conformational search was carried out MM/MD protocol, in which the relaxed structures were subjected to the repeated all the simulation using NVT-MD conditions.

3. Results and Discussion

3.1. Morphological Features

TEM offers a qualitative understanding of the internal structure through direct visualization. Figure 1 shows the results of TEM bright field images of N6CNs of two different magnifications, in which white entities are the cross section of the discrete lamella and the dark area is the nylon 6 matrix due to the staining with 12 tungstophosphoric acid at 80 °C for 2 h. In the enlarged view (Figure 1d), we clearly observe a black exfoliated MMT particle inside the lamella. The lamellar growth occurs on both sides of the dispersed MMT particles, i.e., the mono-layered MMT is sandwiched by the lamella formed. The silicate layers are

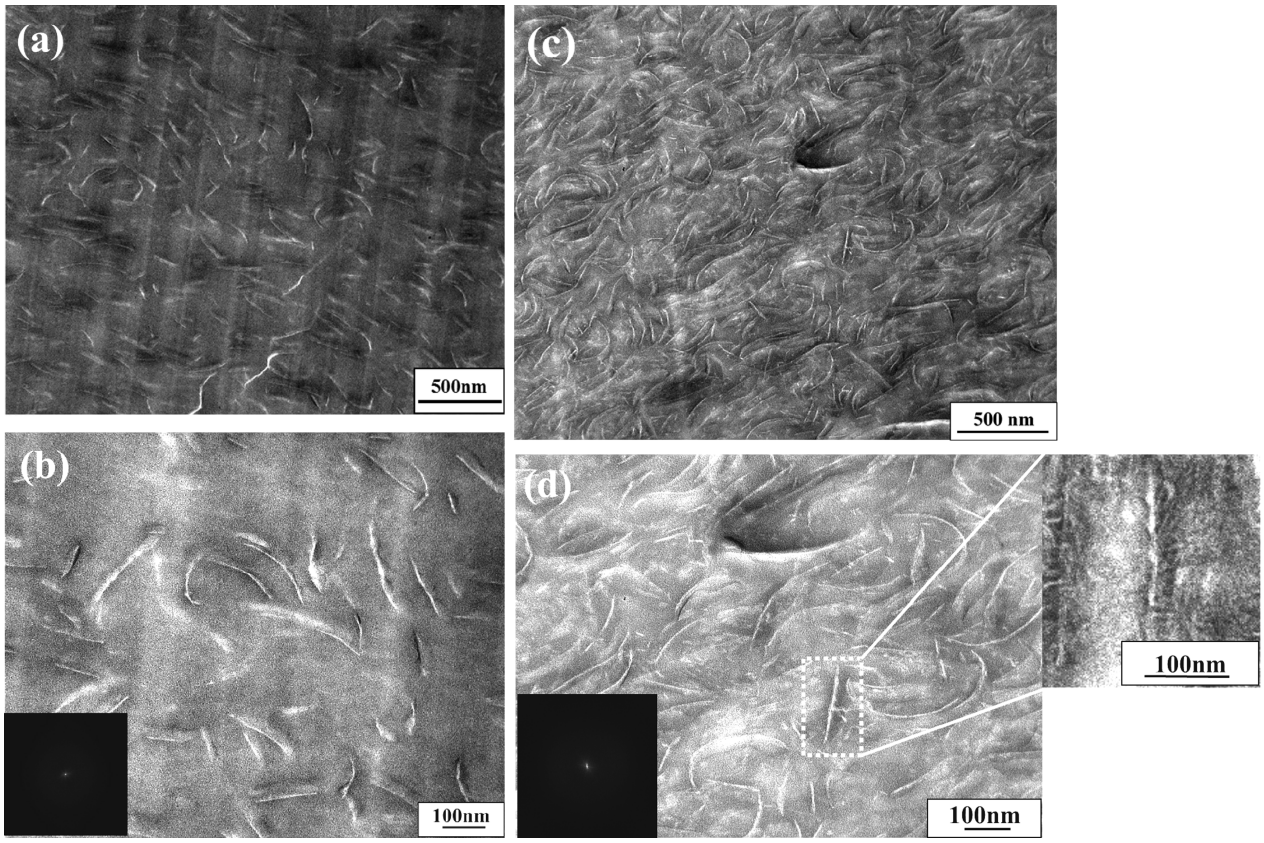

Figure 1. Bright field TEM images of nanocomposites of two different magnifications: (a and b) N6C1.6 and (c and d) N6C3.7. The enlarge part shown (d) forms the indicated lamellae in the original image. The black strip inside the white part is an individual MMT particle. The inset in (b) and (d) are a computed FFT spectrum of the micrograph.

more homogeneously and finely dispersed. The disorder and delaminated layer structure are observed in these TEM images. We estimated the form factors obtained from TEM images, i.e., average value of the particle length (L), curvature ($1/R$) of the dispersed MMT particles, and the correlation length (ξ) between the particles. The details of the evaluation were described in our previous paper.[19] For N6CNs, we have calculated the distribution function of the form factors using the Weibull distribution and the results are presented in Figure 2 and 3. The Weibull function is defined by

$$f(x) = \frac{\alpha}{\beta^{\alpha}} x^{\alpha-1} \exp\left[-\left(\frac{x}{\beta}\right)^{\alpha}\right] \quad (2)$$

where $f(x)$ is the fraction, α and β are the variable numbers. The density of distribution is almost comparative between Gaussian and Weibull fitting curves. The value of β corresponds to average value of the Gaussian distribution.

All factors nicely obeyed the Weibull distribution with the exception of the ξ distribution in N6C3.6. In Figure 3b, the Weibull distribution is compared with the Gaussian distribution. In Table 2, we summarized the form factors obtained from TEM observation. For N6C1.6, L and ξ are maximum in the range of 133 and 91 nm, respectively. With increasing MMT content, N6C3.7 exhibits a small value of L (≅90 nm) accompanied with the narrow distribution, suggesting that a more uniform dispersion of MMT particles seems to be attained as compared to that of N6C1.6. The correlation length between MMT particles ξ (≅26 nm) is smaller than average value of the particle length L (≅90 nm) for N6C3.7, indicating the formation of the highly geometric constraints. That is, the spatial-linked like structure of the dispersed MMT particles is formed. A plausible explanation and its model are presented by Ren et al.[20]. The individual or stacked silicate layers are incapable of freely rotating and hence, by imposing small ω, the relaxation of the structure are prevented almost completely. This type of prevented relaxation leads to the presence of the volume spanning mesoscale network.

At the other interesting feature, the ξ value (≅26 nm) corresponds to the random coil size of nylon 6 in N6C3.7. The root-mean-square radius of gyration $\langle S^2\rangle^{1/2}$ is around 9 nm, which is calculated by $\langle S^2\rangle^{1/2} = 4.0 \times 10^{-2}\ \overline{M}_w^{1/2}$.[21] The

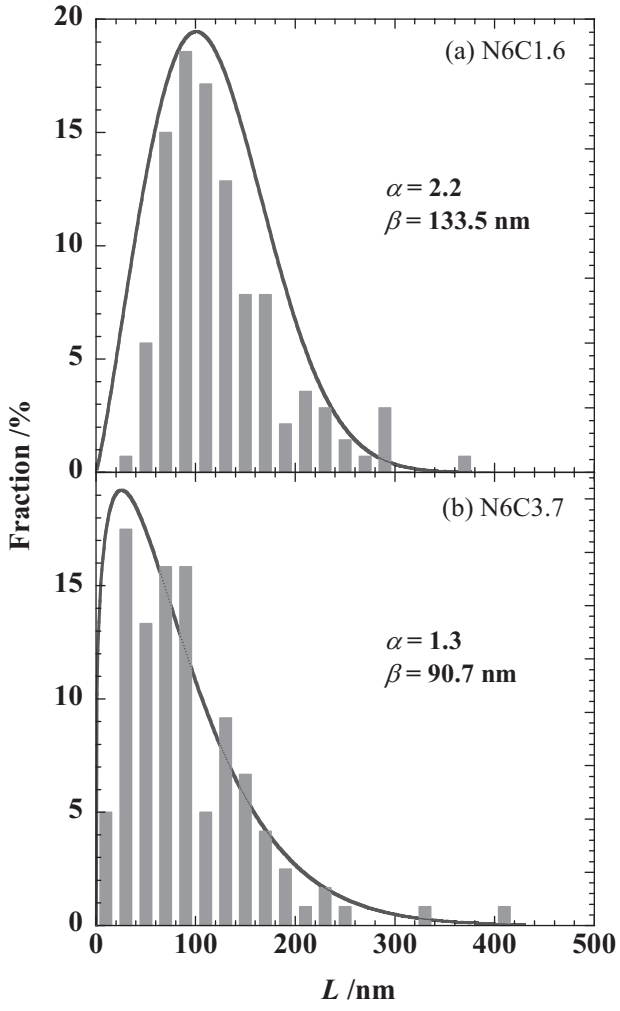

Figure 2. Weibull distribution of particle length (L) for (a) N6C1.6 and (b) N6C3.7.

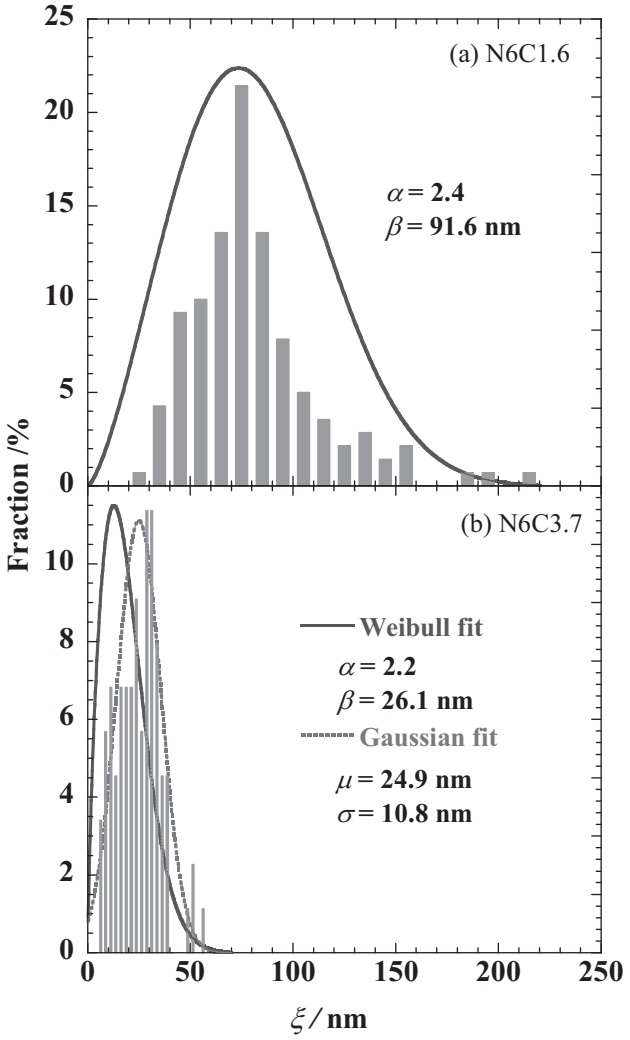

Figure 3. Weibull distribution of correlation length (ξ) between the particles for (a) N6C1.6 and (b) N6C3.7. Average value μ and standard deviation σ in the Gaussian fit through the data are 24.9 and 10.8 nm for N6C3.7, respectively.

chain mobility of the nylon 6 presumably is decreased in translational motion. The morphological difference comes from the loading amount of MMT particles.

3.2. Flexibility of a Single MMT Layer

Two TEM images with two different magnifications are evident for the flexibility of the MMT particles (layers) (Figure 1). When viewed edge-on as in Figure 1, single MMT sheet is apparent as discussed in Section 3.1. The curvature ($1/R$) distribution of the dispersed MMT layers in N6CNs are presented in Figure 4. The obtained value of $1/R$ ($\cong 8 \times 10^{-3}\,\mathrm{nm}^{-1}$) for N6C3.7 exhibits a large degree of flexibility of the mono-layered MMT sheet. It is well known that smectite clay sheet have a large degree of flexibility.[22] Sato et al.[23] reported the study of the flexibility of smectite clay minerals by using MD simulations. They took into account the quantitative understanding of the mechanical behavior of a single clay layer in a completely exfoliated state. The repeating unit of a layer is taken to be $a_0 = 0.52$ nm and $b_0 = 0.902$ nm with formula of $2Na_{1/3}(Si_{11/3}Al_{1/3})Al_2O_{10}(OH)_2$ which corresponds to that of beidellite. When the size of the basic cell ($A = 9.3$ nm,

Table 2. Morphological parameters of nanocomposites obtained from TEM analysis.

Sample	L [nm]	ξ [nm]	$1000/R$ [nm^{-1}]
N6C1.6	133.5	91.6	4.8
N6C3.7	90.7	26.1	7.9

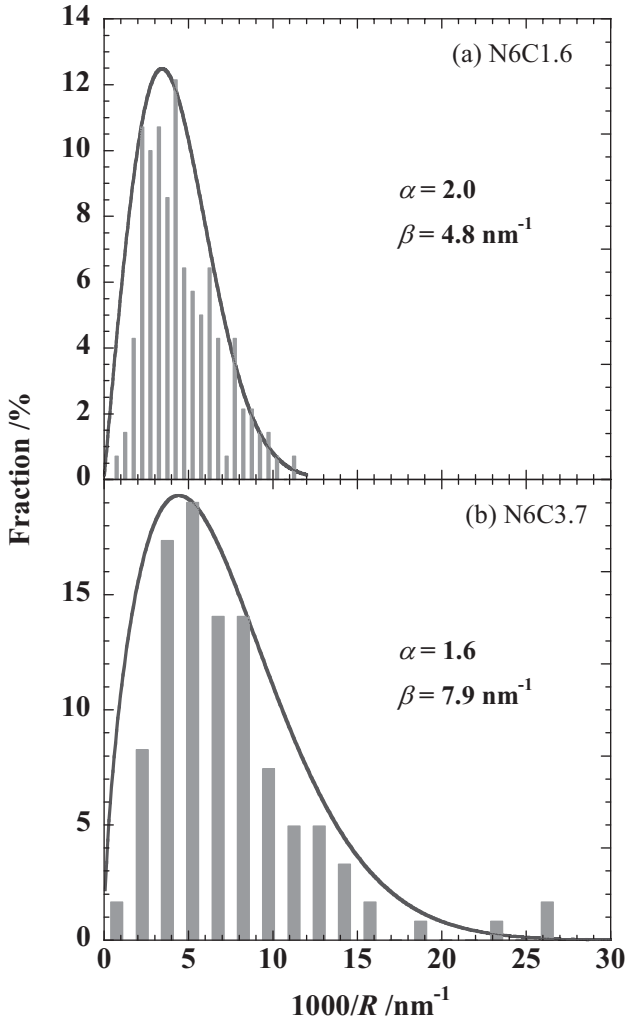

Figure 4. Weibull distribution of curvature (1/*R*) for (a) N6C1.6 and (b) N6C3.7.

$B = 2.6$ nm, and $C = 5$ nm) (A-type cell) is reduced by 3–40% in the *A*-direction, the stationary structure of a clay layer is obtained as a curved sheet with a 2:1 smectite-type layer. In such curved state, the layer experiences a external stress of 0.5–0.7 GPa. The layer structure of a clay fractures when the size of the same basic cell is reduced by more than 40%. This value is much lower than that of moscovite (≈2 GPa) which is also reported by same authors.[24] The simulation has also done by reducing the size of the basic cell ($A = 3.1$ nm, $B = 10.7$ nm, and $C = 5$ nm) (B-type) in the *B*-direction. The clay layer is found to be more flexible along the *A*-direction than along the *B*-direction. When the microscopic structure of a curved clay layer is examined, it is concluded that the main origin of the flexibility lies in the change of Si–O–Si angle in the silicate tetrahedral sheets rather than in the change of bond lengths. These simulation results agree with the atomic force microscopy (AFM) observations.[25]

3.3. Volume Spanning Mesoscale Network

The inset in Figure 1b and d is a computed FFT patterns of the corresponding TEM micrographs. Figure 5a shows the one-dimensional scattering pattern obtained from FFT analysis. Here, the scattering intensity [$I(q)$] is shown as a function of the magnitude of the scattering vector (q). We found small remnant peaks in the q range from 0.02 to 0.3 nm^{-1}. The broadness is due to the fact that the dispersed MMT particles are rather disordered and short-range ordered. The decay of intensity in the q range from 0.3 to 0.1 nm^{-1} can be expected by a power law in the form $I(q) \cong q^{-1}$, suggesting the form factor is the randomly oriented rod. Apparently, this is consistent with the shape of the dispersed MMT particles in the TEM image (Figure 1).

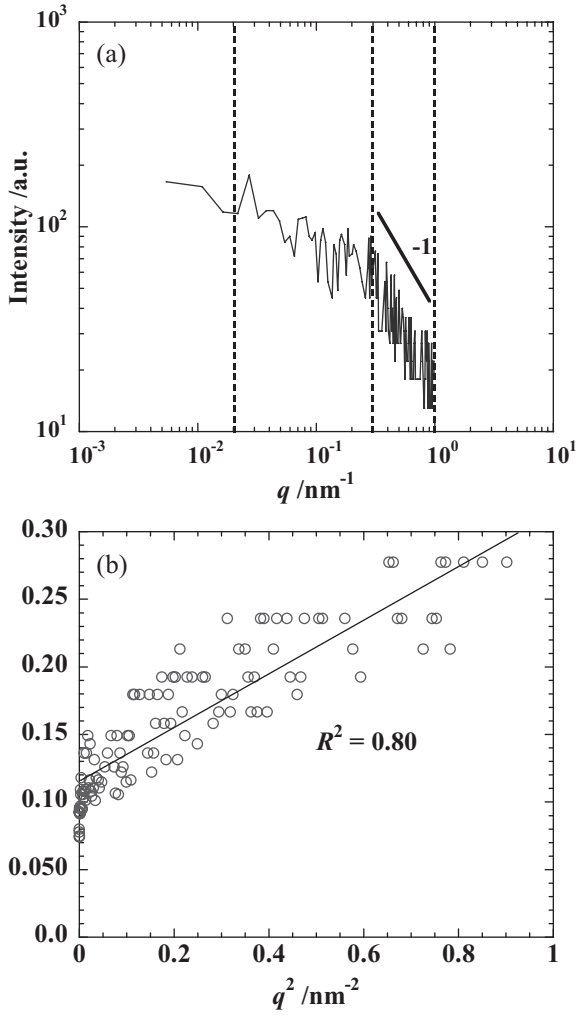

Figure 5. (a) One-dimensional scattering pattern of N6C3.7 obtained from FFT analysis. The solid line was drawn by the power low of $I(q) \cong q^{-1}$ at the q range of 0.02–0.3 nm^{-1}. (b) Debye-Bueche plot for FFT analysis. The solid line is calculated by linear regression.

We estimated the form factors obtained from TEM images and FFT analysis combined with Debye-Bueche (DB) theory, i.e., average value of the particle thickness (t_{MMT}) of the dispersed particle and the correlation length (ξ_{MMT}) between the particles. The Debye-Bueche equation[26] is applicable in isotropic dense system.[27] The detail procedure for the Debye-Bueche plots was described in our previous paper.[28] To estimate these values, we employed the Debye-Bueche equation:

$$I(q)^{1/2} = \frac{(8\pi\langle\rho^2\rangle\varsigma^3)^{1/2}}{(1+\varsigma^2q^2)} \quad (3)$$

where ζ is the long-range structure correlation distance, q is the magnitude of scattering vector, $I(q)$ is the intensity of the scattered light at q, and $\langle\rho^2\rangle$ is the mean-square fluctuation of the refractive index.[29]

Figure 5b shows the Debye-Bueche plot for FFT analysis. The plot is observed to be linear. From the slope and the intercept, we can estimate ζ (=slope/intercept)$^{1/2}$. Once the value of ζ (=1.14 nm) is given, other morphological parameters are obtained from

$$\xi_{MMT} = \frac{\varsigma}{\phi_{MMT}} \quad (4)$$

$$t_{MMT} = \frac{\varsigma}{1-\phi_{MMT}} \quad (5)$$

where ϕ_{MMT} is the volume fraction of the dispersed phase (MMT particles). The details of the evaluation were described in our previous paper.[28] The results are presented in Table 3.

For N6C1.6, ξ_{MMT} and t_{MMT} are 108.6 and 0.8 nm, respectively. On the other hand, N6C3.7 exhibits a large value of ξ_{MMT} (67.5 nm), which is almost double as compared with that of TEM observation ($\xi = 26.1$ nm). The reason is not obvious at present. However, the absolute value of t_{MMT} in each N6CN shows the same value of the mono-layer thickness of MMT (t^*_{MMT}= 0.96 nm[30]). The mono-layered MMT sheets are finely dispersed into nylon 6 matrix. Since both values of t_{MMT} for N6CN were virtually same, we have estimated the aspect ratio (L/t^*_{MMT}) by considering the value of t_{MMT} to be equal to 0.96 nm.

Between 1.6 and 3.7 wt% (ϕ_{MMT} between 0.72 and 1.69) MMT, a percolation threshold value for the formation of the volume spanning mesoscale network exists, and we can control the network formation and hence various properties. We may explain this with the help of classical rheological theory of suspension of conventional filler reinforced systems.[31] The rotation of filler is possible when $\phi_{filler} < \phi_{critical} \cong (\text{aspect ratio})^{-1}$. For N6C3.7 this relation is not valid, in which $100\phi_{MMT} = 1.69 > 1.10$ [$\sim 100(L/t^*_{MMT})^{-1}$] (Table 3). For this reason in N6C3.7, the rotation of mono-layered MMT in the nylon 6 matrix is completely hindered. At the same time, the pseudo-solid like behavior is generated in N6C3.7. This behavior is clearly observed in dynamic storage modulus measurements under molten state (Figure 6).

Table 3. Form factors of nanocomposites obtained from TEM and FFT analyses.

Sample	100 ϕ_{MMT}	ξ_{MMT} [nm]	t_{MMT} [nm]	100 $(L/t^*_{MMT})^{-1}$
N6C1.6	0.723	108.6	0.8	0.72
N6C3.7	1.69	67.45	1.1	1.06

3.4. Melt Rheology

The flow behavior of N6CNs differed extremely from that of the corresponding neat matrix, whereas the thermo-rheological properties of the nanocomposites were entirely

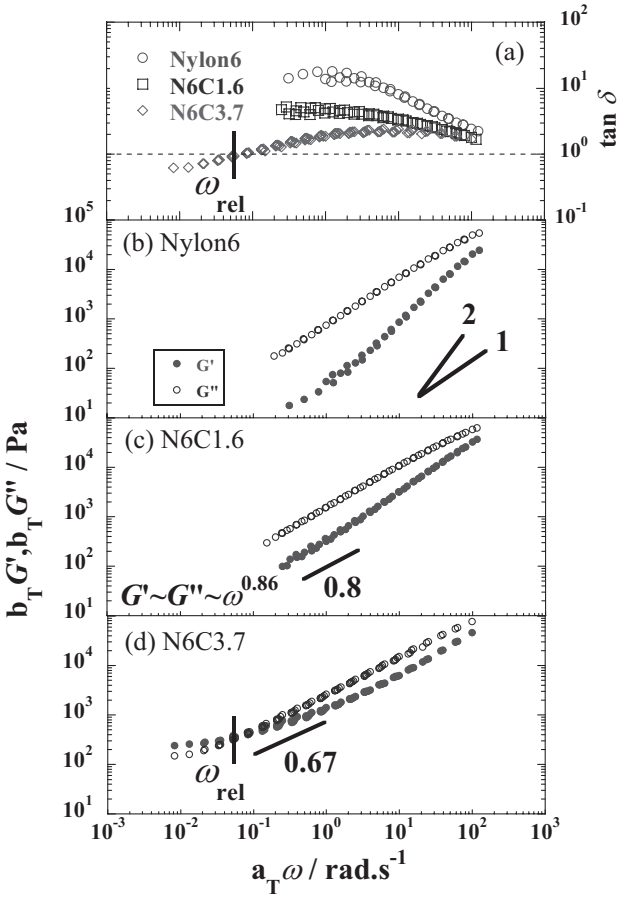

Figure 6. Reduced frequency dependence of (a) tan δ, storage modulus $G'(\omega)$ and loss modulus $G''(\omega)$ of (b) neat nylon 6, (c) N6C1.6, and (d) N6C3.7 at $T_r = 225$ °C. The solid line was drawn by the power low of $G'(\omega) \approx G''(\omega) \propto \omega^{0.8}$ in the low-ω region for N6C1.6.

determined by that behavior of matrix.[32] The slope of $G'(\omega)$ and $G''(\omega)$ versus the $a_T\omega$ is much smaller than 2 and 1, respectively. Values of 2 and 1 are expected for linear monodispersed polymer melts, where the polymer chains should be fully relaxed. A large deviation especially in the presence of very small amount of MMT loading may be due to the formation of network structure in the melt state.[33] The temperature dependence frequency shift factor (a_T, Arrhenius-type) were used to generate master curves. The shift factor b_T shows large deviation from a simple density effect, it would be expected that the values would not vary far from unity ($b_T = \rho T/\rho_r T_r$, where ρ and ρ_r are the density at T and T_r, respectively).[34,35] One possible explanation is a network structural change occurring in N6CNs during measurement (shear process). The reconstituting of the percolated MMT network probably supports for the melt under weak shear flow (terminal zone), thereby leads to the increase in the absolute values of $G'(\omega)$ and $G''(\omega)$.[35]

As seen in Figure 6, in the linear viscoelastic regime, a big change in terminal (low frequency $a_T\,\omega < 3$ rad s^{-1}) region from liquid-like response to a solid-like response was observed for N6C1.6 [$G'(\omega) \approx G''(\omega) \propto \omega^{0.86}$], ascribed to the weak formation of a volume spanning mesoscale MMT network (gel point).[36] The terminal rheology is sensitive to MMT loading and extent of exfoliation in the polymer matrix. For N6C3.7, at low frequency ($a_T\omega < 1$ rad s^{-1}), both moduli exhibit weak ω-dependence [$G'(\omega) \approx G''(\omega) \propto \omega^{0.67}$] accompanied with the cross over frequency ω_{rel}, which is determined from the measured master curve when tan δ is unity. The results of the temperature dependence of relaxation rate (ω_{rel}), assuming that the rate is of Arrhenius-type. The activation energy of the relaxation of the network is estimated to be 152 kJ mol^{-1} in the range of temperature between 225 and 255 °C.[35]

Figure 7 represents the MMT content dependent (ϕ_{MMT}) flow activation energy (E_a) of nylon 6 and various N6CNs having different ϕ_{MMT}. We investigated the low frequency values of complex viscosity ($|\eta^*|$) as a function of temperature in each system. At temperature where a zero-shear value was not obtained experimentally, a combination of time-temperature superposition and best fit using the Ellis model was employed to obtain a zero-shear viscosity ($|\eta_0^*|$) from a master curve. The values are calculated from Arrhenius-type equation given as $|\eta_0^*| \propto \exp(E_a/RT)$. It is clearly observed that E_a value systematically increases with increasing MMT content up to ϕ_{MMT} is equal to 0.013. On a further increase of MMT content, E_a value suddenly increases with a very high value of 43.0 kJ mol^{-1}, which means with high MMT content it is very difficult for the materials to flow. This behavior also ascribed to the formation of volume spanning mesoscale MMT network in N6C3.7 with high MMT content under molten state. The value of ϕ_{MMT} between 0.013 and 0.014 is the percolation threshold value for such strong network formation in case of N6CNs.

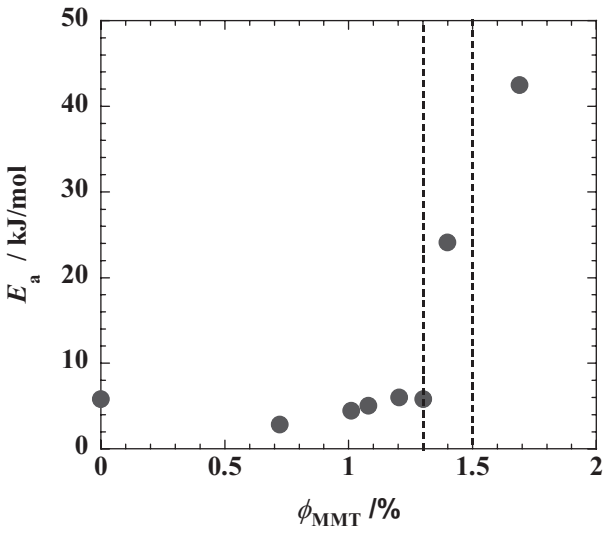

Figure 7. Flow activation energy (E_a) as a function of MMT content (ϕ_{MMT}).

Another interesting feature is that the activation energy of the relaxation of the network exhibits large value one order higher in magnitude compared with the flow activation energy of N6C3.7, so that the liquid-like response might be overwhelmed.

3.5. Dynamic Mechanical Properties

Dynamic mechanical analysis measures the response of a given material to a cyclic deformation (here in tension-torsion mode) as a function of temperature. DMA results are expressed by three main parameters: (a) the storage modulus (G') corresponding to the elastic response to the deformation; (b) the loss modulus (G''), corresponding to the plastic response to the deformation, and (c) tan δ, that is the (G''/G') ratio, useful for determining the occurrence of molecular mobility transitions such as the glass transition temperature (T_g).

At the temperature range of −150–0 °C, there is a maximum of 170–240% increment of G' for N6CNs in comparison to that of the matrix at well below T_g. Above T_g, when materials become soft the reinforcement effect of MMT particles becomes prominent, due to the restricted movement of the polymer chains, and hence strong enhancement (≈400%) of modulus appeared (data not shown). This behavior is common for the nanocomposites reported so far.[1]

Figure 8 shows the effect of MMT content on T_g of matrix polymer, represented by the tan δ peak location at the temperature range of 0–100 °C. Other two peaks in tan δ curves are observed at the range of temperature between

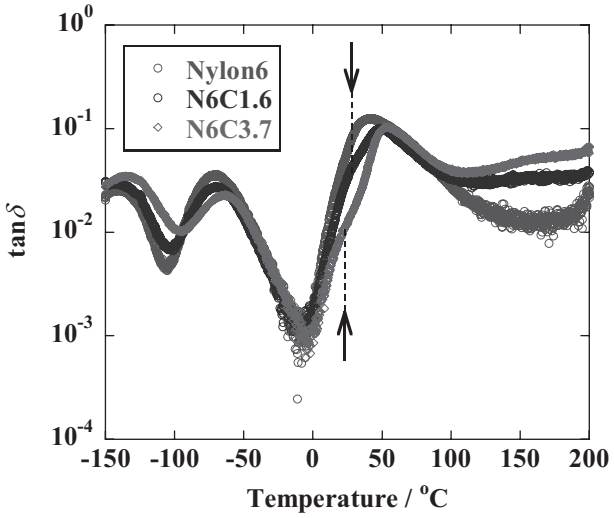

Figure 8. Temperature dependence of tan δ for neat nylon 6 and nanocomposites.

−100 and −50 °C and at low temperature around −140 °C as a third peak, respectively. The former corresponds to the local motion of the amide groups possessing the formation of rather weak hydrogen bonding between amorphous chains, which is defined as β-relaxation. The latter corresponds to the local motion of the methylene (CH_2) segments, which is defined as γ-relaxation.[37]

For T_g of matrix nylon 6, the presence of MMT particles leads to a significant peak shift to higher temperature accompanied with the depression of peak height of the tan δ curves for N6CNs compared to that of pure nylon 6. At the same time, a small remnant shoulder is observed around 20 °C (marked with the arrows). The magnitude of the shift estimated by tan δ is about 12 °C. The suppression of the glass transition (increase of T_g) may be ascribed to the restricted segmental motions at the nylon 6/MMT interfaces neighborhood of the exfoliated N6CNs. The β-relaxation exhibits same trend with loading of MMT. At the same time, the reduction of the thermal expansion coefficient (α) at the temperature range of −150–20 °C in N6CNs seems to stem from the mechanical constraint by the dispersed MMT particles. N6CNs show significant reduction of α value and the value decreases up to ≈ 20% for N6C3.7 as compared with that of neat nylon 6 (Table 1).

At the temperature range between 100 and 200 °C, the increasing of tan δ is due to the dampening effect of the MMT particles, as seen by the larger values of G'' in this region.

3.6. Molecular Dynamics (MD) Simulation

To understand the generic dynamic rheology in terms of the restricted segmental motions at the nylon 6/MMT interfaces neighborhood, we conducted NVT-MD simulation. For the generation of accurate model amorphous structures for nylon 6, the constitutive repeating unit (CRU) was built and its geometry optimized by energy minimization. The CRU was polymerized to a conventional degree of polymerization ($\overline{DP}_n$) equal to 10. Although this chain may be too short to capture the genuine response of a long nylon 6 molecule, in the case of polystyrene (PS) it has been verified that a polymer with same $\overline{DP}_n$ is longer than average persistence length of PS in PS-based PCNs.[38] MMT consists of an octahedral $AlO_4(OH)_2$ sheet sandwiched between two SiO_4 tetrahedral layers (of ≈1 nm thick and ≈100 nm diameter) with the charges being adjusted by substituting Al^{3+} or Si^{4+} with Mg^{2+} and the depressed charges being neutralized with alkaline cations intercalated into the interlayer spaces to form a laminate structure of several layers. The chemical formula was $Na_{0.66}(Al_{3.34}Mg_{0.66})Si_8O_{20}(OH)_4$ having cation exchange capacity of 87 mequiv. $(100\,g)^{-1}$ [1] (as reported by the supplier, Nanocor Inc.). From these results, we can estimate the surface charge density, which is calculated to be $-0.780e$ nm^{-2}. This estimation assumes that the negative charges are evenly distributed in a cubic array over the MMT surface and that half of the charges are located on the one side of the platelet and the other half reside on the other side. Furthermore, the surface hydroxy concentration of MMT was estimated by titration with triethyl aluminum. The calculated value of a Si−OH density was 5(Si−OH) nm^{-2}.[39] That is, 500 OH groups are localized near the edge surface of the individial silicate layers ($\approx 1 \times 100$ nm^2). These OH groups are particularly important because it improves the strength of the interface between nylon 6 matrix and MMT. For this reason, silica tetrahedral terminated with OH [$Si(OH)_4$] was modeled instead of layered silicate MMT, and overall system was built. For comparison, 50 ε-aminocaproicacid monomers were used as a reference.To illustrate the molecular conformations near $Si(OH)_4$ molecule, we reported two snapshots (Figure 9) taken from a MD simulation for 10 ps at 298 K of the system made up by nylon 6 molecule ($\overline{DP}_n = 10$) of 5 chains/50 $Si(OH)_4$ molecules and 50 monomers/50 $Si(OH)_4$ molecules. Figure 10 and 11 show the time variation of the energy components for the simulation shown in Figure 9. From the equilibrium conformation of the corresponding system we calculated the total energy of a system, which may be composed by the potential and kinetic energies. The results are presented in Table 4. The large value of the total energy appeared in nylon 6 molecules as compared with that of the system in monomers. The potential energy in $Si(OH)_4$ molecules decreases in almost linear fashion with increasing molecules in the system. The interesting feature is the variation of the total energy generated in the systems when the system incorporates $Si(OH)_4$ molecule up to 50 units. The

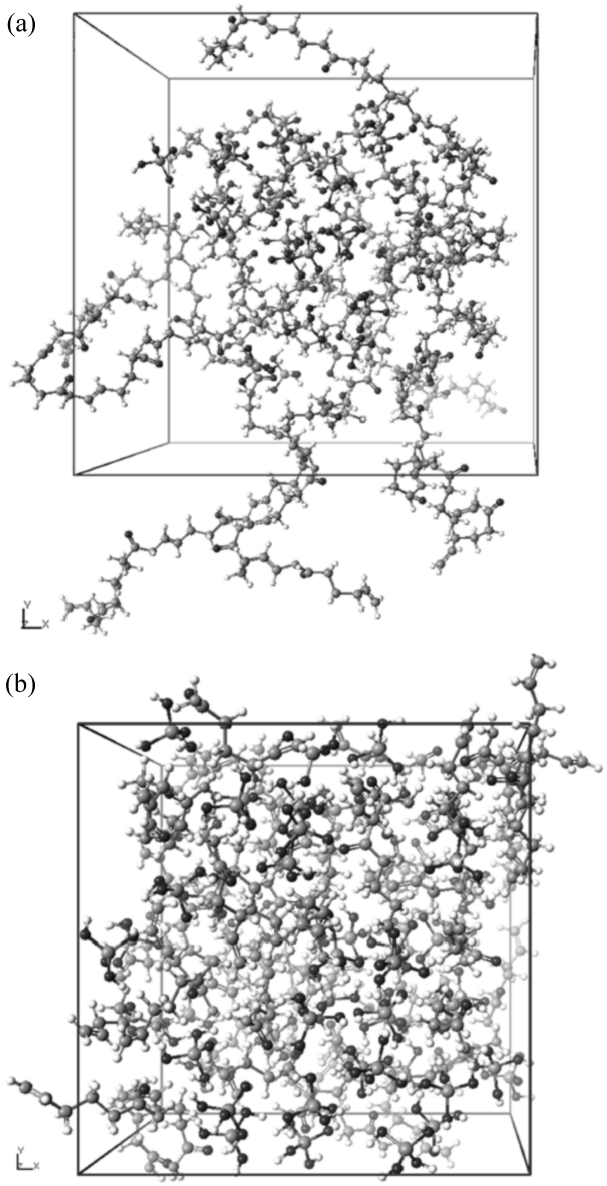

Figure 9. Two snapshots extracted from MD trajectory at 298 K of a system comprising (a) nylon 6 molecule ($\overline{DP}_n = 10$) of 5 chains/50 $Si(OH)_4$ molecules and (b) 50 monomers/50 $Si(OH)_4$ molecules.

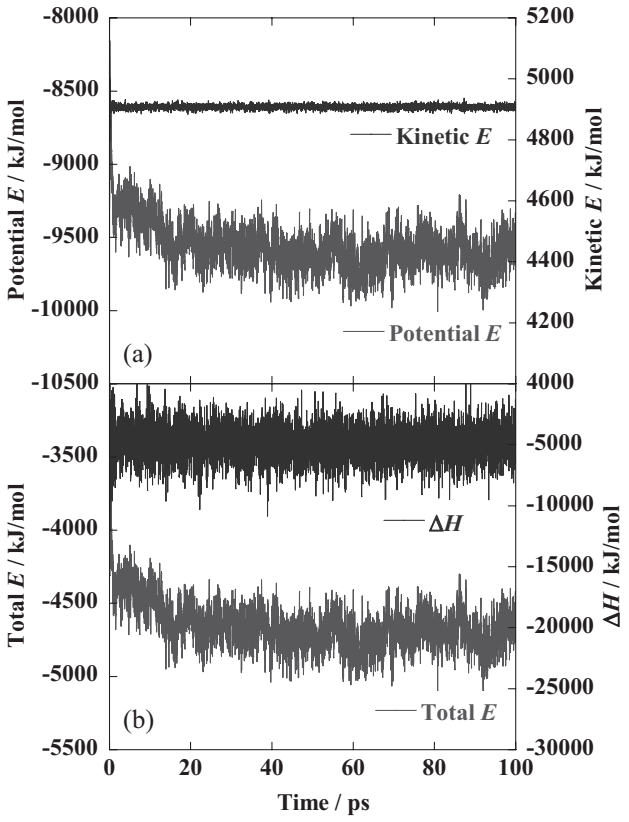

Figure 10. Profiles of the energy components for the simulation of nylon 6 molecules/$Si(OH)_4$ molecules as shown in Figure 9a: (a) potential and kinetic energies and (b) total energy and enthalpy.

incorporation of $Si(OH)_4$ molecules induces the reduction of the total energy accompanied with decreasing of the enthalpy due to the negative potential energy of $Si(OH)_4$ molecules. The enthalpy having extremely large negative value ($-5000\,kJ\,mol^{-1}$) is evident in nylon 6/50 $Si(OH)_4$ molecules as compared with the system of monomers/$Si(OH)_4$ molecules ($40\,000\,kJ\,mol^{-1}$). Therefore it can be assumed that the OH groups induce the strong interfacial interaction between nylon 6 molecules and $Si(OH)_4$ molecules. We can speculate the restricted segmental motions at the nylon 6/MMT interfaces neighborhood of the exfoliated N6CNs as discussed in Section 3.5.

4. Conclusion

In this study, we have inferred the existence of percolated clay network structure in N6CNs through TEM and FFT analyses. The volume fraction of MMT between 0.013 and 0.014 was the percolation threshold value for strong network formation. For N6C3.7, the volume spanning MMT network led to a very high value of the flow activation energy as compared with that of neat nylon 6, resulting in the pseudo-solid like response under molten state. The dispersed mono-layered MMT sheets strongly contributed toward the enhancement of the dynamic storage and loss moduli, leading to the suppression of the glass transition. The magnitude of the shift estimated by tan δ was about 12 °C for N6C3.7 due to restricted segmental motions at the nylon 6/MMT interfaces neighborhood of the exfoliated nanocomposite. We have discussed the nylon 6 molecules in confined environment by NVT-MD simulation. The

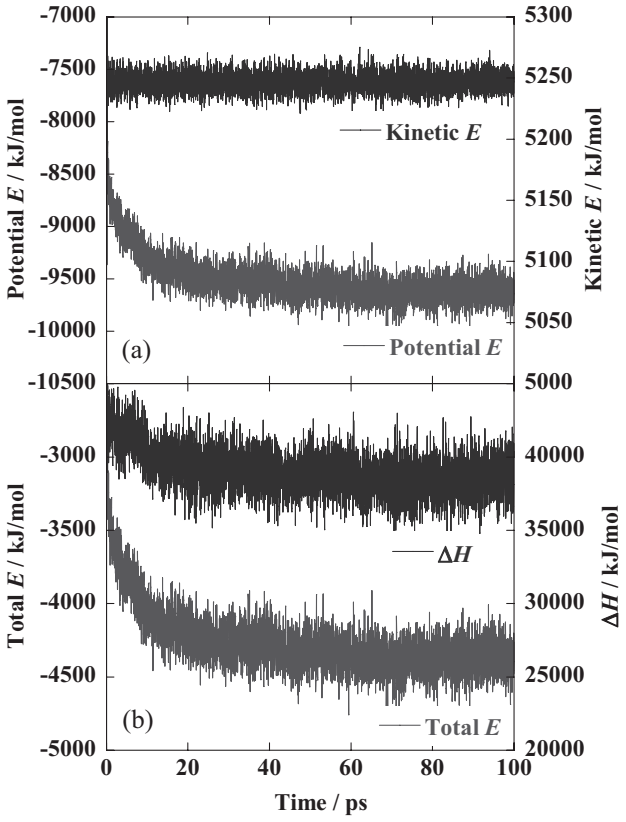

Figure 11. Profiles of the energy components for the simulation of monomers/$Si(OH)_4$ molecules as shown in Figure 9b: (a) potential and kinetic energies and (b) total energy and enthalpy.

incorporation of $Si(OH)_4$ molecules into the system made up by nylon 6 molecules/$Si(OH)_4$ molecules induced the reduction of the total energy accompanied with decreasing of the enthalpy due to the negative potential energy of $Si(OH)_4$-molecules. The formation of the strong interfacial interaction between nylon 6 molecules and $Si(OH)_4$ molecules induced by OH groups was suggested.

Acknowledgements: This work was supported by the Strategic Research Infrastructure Project of the Ministry of Education, Sports, Science, and Technology, Japan (2010-2014).

Received: February 24, 2012; Revised: April 10, 2012; Published online: August 2, 2012; DOI: 10.1002/mame.201200065

Keywords: molecular dynamics simulations; nanocomposites; percolated clay networks; rheology

[1] S. Sinha Ray, M. Okamoto, *Prog. Polym. Sci.* **2003**, *28*, 1539.
[2] R. A. Vaia, H. D. Wagner, *Mater. Today* **2004**, *7*, 32.
[3] F. Gao, *Mater. Today* **2004**, *7*, 50.
[4] M. Okamoto, *Mater. Sci. Technol.* **2006**, *22*, 756.
[5] A. Okada, A. Usuki, *Macromol. Mater. Eng.* **2006**, *291*, 1449.
[6] F. Hussain, M. Hojjati, M. Okamoto, R. E. Gorga, *J. Compos. Mater.* **2006**, *40*, 1511.
[7] A. Usuki, A. Y. Kojima, A. Okada, Y. Fukushima, T. Kurauchi, O. Kamigaito, *J. Mater. Res.* **1993**, *8*, 1174.
[8] R. A. Vaia, E. P. Giannelis, *Macromolecules* **1997**, *30*, 8000.
[9] R. Krishnamoorti, R. A. Vaia, E. P. Giannelis, *Chem. Mater.* **1996**, *8*, 1728.

Table 4. Energy components and enthalpy calculated from simulation of systems.

Systems	Energy components [kJ mol^{-1}]			Enthalpy [kJ mol^{-1}]
	Potential	Kinetic	Total	
nylon 6 (five chains, $\overline{DP}_n = 10$)	3800	3200	7000	6500
50 monomers	2200	3500	5600	19 000
$Si(OH)_4$ (5 molecules)	−900	170	−700	3000
$Si(OH)_4$ (10 molecules)	−1750	330	−1400	6000
$Si(OH)_4$ (30 molecules)	−5800	1000	−4800	15 000
$Si(OH)_4$ (50 molecules)	−10 000	1650	−8500	25 000
nylon 6/$Si(OH)_4$ (5)	2300	3350	5700	6000
nylon 6/$Si(OH)_4$ (10)	1200	3500	4700	5000
nylon 6/$Si(OH)_4$ (30)	−4000	4200	100	0
nylon 6/$Si(OH)_4$ (50)	−9500	4900	−4600	−5000
50 monomers/$Si(OH)_4$ (5)	10 000	3700	13 500	95 000
50 monomers/$Si(OH)_4$ (10)	7300	3850	11 000	83 000
50 monomers/$Si(OH)_4$ (30)	−2000	4500	2700	55 000
50 monomers/$Si(OH)_4$ (50)	−9500	5200	−4300	38 000

[10] Y. Rao, J. M. Pochan, *Macromolecules* **2007**, *40*, 290.
[11] M. A. Treece, J. P. Oberhauser, *Macromolecules* **2007**, *40*, 571.
[12] P. Sollich, F. Lequeux, P. Hebraud, M. E. Cate, *Phys. Rev. Lett.* **1997**, *78*, 2020.
[13] J. Ren, B. F. Casanueva, C. A. Mitchell, R. Krishnamoorti, *Macromolecules* **2003**, *36*, 4188.
[14] H. Tanaka, J. Meunier, D. Bonn, *Phys Rev. E* **2004**, *69*, 031404.
[15] P. Maiti, M. Okamoto, *Macromol. Mater. Eng.* **2003**, *288*, 440.
[16] Y. H. Kim, M. Okamoto, T. Kotaka, *Macromolecules* **2000**, *33*, 8114.
[17] P. H. Nam, P. Maiti, M. Okamoto, T. Kotaka, N. Hasegawa, A. Usuki, *Polymer* **2001**, *42*, 9633.
[18] K. H. Illers, *Makromol. Chem.* **1978**, *179*, 497.
[19] S. Sinha Ray, K. Yamada, M. Okamoto, A. Ogami, K. Ueda, *Chem. Mater.* **2003**, *15*, 1456.
[20] J. Ren, A. S. Silva, R. Krishnamoorti, *Macromolecules* **2000**, *33*, 3739.
[21] S. H. Anastasiadis, T. P. Russel, S. K. Satija, C. F. Majkrzak, *J. Chem. Phys.* **1990**, *92*, 5677.
[22] K. A. Carrado, in: *Handbook of Layered Materials* (Eds: S. M. Auerbach, K. A. Carrado, P. K. Dutta), Marcel Dekker, New York **2004**, p. 1.
[23] H. Sato, A. Yamagishi, K. Kawamura, *J. Phys. Chem B* **2001**, *105*, 7990.
[24] Y.-S. Seo, Y. Ichikawa, K. Kawamura, *Mater. Sci. Res. Int.* **1999**, *5*, 13.
[25] K. Tamura, H. Setsuda, M. Taniguchi, A. Yamagishi, *Langmuir* **1999**, *15*, 6915.
[26] P. Debye, A. M. Bueche, *J. Appl. Phys.* **1949**, *20*, 518.
[27] B. S. Hsiao, R. S. Stein, K. Deutscher, H. H. Winter, *J. Polym. Phys.* **1990**, *28*, 1571.
[28] M. Okamoto, T. Inoue, *Polym. Eng. Sci.* **1993**, *33*, 175.
[29] M. Okamoto, T. Inoue, *Polymer* **1995**, *36*, 2736.
[30] G. Lagaly, *Clay Miner.* **1970**, *16*, 1.
[31] L. A. Utracki, *Polymer Alloya and Blends: Thermodynamics and Rheology*, Hasser Publishers, New York **1990**.
[32] R. Krishnamoorti, E. P. Giannelis, *Macromolecules* **1997**, *30*, 4097.
[33] S. Sinha Ray, K. Yamada, M. Okamoto, K. Ueda, *Polymer* **2003**, *44*, 6631.
[34] M. L. Williams, R. F. Landel, J. D. Ferry, *J. Am. Chem. Soc.* **1955**, *77*, 3701.
[35] Y. Katoh, M. Okamoto, *Polymer* **2009**, *50*, 4718.
[36] J. E. Martin, D. Adolf, J. P. Wilcoxon, *Phys. Rev.* **1989**, *A39*, 1325.
[37] A. E. Woodward, J. M. Crissman, J. A. Sauer, *J. Polym. Sci.* **1960**, *44*, 23.
[38] E. Manias, V. Kuppa, in: *Polymer Nanocomposite ACS Symposium Series*, Vol. 804 (Eds: R. Vaia, R. Krishnamoorti), Oxford University Press, Oxford **2002**, p. 193.
[39] M. C. Hermosin, J. Cornejo, *Clay Miner.* **1986**, *34*, 591.